

RESEARCH ARTICLE

10.1002/2015WR017286

Key Points:

- LCL crossing and CAPE threshold define four convective regimes
- Atmosphere with earlier LCL crossings does not imply larger CAPE
- CAPE tends to be larger in wetter soil conditions

Correspondence to:

A. Porporato,
amilcare.porporato@duke.edu

Citation:

Yin, J., J. D. Albertson, J. R. Rigby, and A. Porporato (2015), Land and atmospheric controls on initiation and intensity of moist convection: CAPE dynamics and LCL crossings, *Water Resour. Res.*, 51, 8476–8493, doi:10.1002/2015WR017286.

Received 24 MAR 2015

Accepted 7 OCT 2015

Accepted article online 11 OCT 2015

Published online 28 OCT 2015

Land and atmospheric controls on initiation and intensity of moist convection: CAPE dynamics and LCL crossings

Jun Yin¹, John D. Albertson^{1,2}, James R. Rigby³, and Amilcare Porporato¹

¹Department of Civil and Environmental Engineering, Pratt School of Engineering, Duke University, Durham, North Carolina, USA, ²School of Civil and Environmental Engineering, Cornell University, Ithaca, New York, USA, ³USDA-ARS National Sedimentation Laboratory, Oxford, Mississippi, USA

Abstract The local role that land-atmosphere interactions play in the rainfall process has been often explored by investigating the initiation of moist convection as the top of the atmospheric boundary layer (ABL) crosses the lifting condensation level (LCL). However, this LCL crossing alone is not a sufficient indicator of the probability and intensity of subsequent convective precipitation, which is instead better characterized by the added consideration of the so-called convective available potential energy (CAPE). In this study, both the LCL crossing and CAPE are jointly considered as the primary indicators of the occurrence and intensity of moist convection in order to analyze the land-atmosphere interactions through a simple soil-plant system and a zero-dimensional mixed-layer model. The approach is explored using the free atmospheric conditions observed at the Central Facility in the Southern Great Plains, where the ABL analysis shows both dry and wet soil can be conducive to early moist convection depending on atmospheric conditions but CAPE always tends to be larger under wetter soil conditions. The combination of the two indicators, LCL crossing and CAPE, further allows us to classify free atmosphere and soil moisture regimes into positive and negative feedback regimes for moist convection.

1. Introduction

Land-atmosphere coupling involves interacting processes among surface and subsurface hydrology, vegetation, and atmospheric dynamics at different spatial and temporal scales [Ek and Mahrt, 1994; Brubaker and Entekhabi, 1995; D'Odorico and Porporato, 2004; Scanlon and Albertson, 2004; Qian et al., 2013; Ford et al., 2014]. In particular, the soil water content, surface albedo, and magnitude of surface energy fluxes affect the dynamics of the boundary layer, while the atmospheric conditions influence the surface evapotranspiration via environmental factors, such as radiative forcing, temperature, wind speed, vapor pressure deficit, and CO₂ concentration. These factors form interesting feedback loops that control the relationships between surface hydrology and atmospheric moist convection, and in turn play an important role in climatic and ecohydrological processes [Betts et al., 1996; Findell and Eltahir, 2003; Koster et al., 2003; Juang et al., 2007a; Betts, 2009; Siqueira et al., 2009; Konings et al., 2010; Yin et al., 2014].

Several previous studies have analyzed the land surface and free atmospheric controls on the initiation of moist convection and cloud formation focusing on the conditions leading the atmospheric boundary layer (ABL) to cross the lifting condensation level (LCL) [Ek and Mahrt, 1994; Ek and Holtslag, 2004; Juang et al., 2007a, 2007b; Konings et al., 2010; Gentine et al., 2013]. In particular, simple mixed-layer models of the ABL have been effective in capturing these processes and elucidating the connection between the surface states and the ABL growth toward the LCL. For example, Siqueira et al. [2009] explored the linkage between soil moisture and initiation of moist convection by coupling a soil-plant hydrodynamics model to a simplified ABL model and found that when the soil is dry an external source of water (i.e., advection) is required to trigger moist convection. Gentine et al. [2013] found dry soil advantage and wet soil advantage regimes by investigating the relative humidity at the top of the boundary layer through a conceptual mixed-layer model.

It is important to note that the LCL crossing is a necessary but not sufficient condition for the initiation of deep convection. This is demonstrated, e.g., in the modeling study of Juang et al. [2007a] where convective precipitation was always preceded by LCL crossing, while convective precipitation only occurred in 45% of the LCL crossing cases. The reason for this is that the probabilities of occurrence and intensity of moist

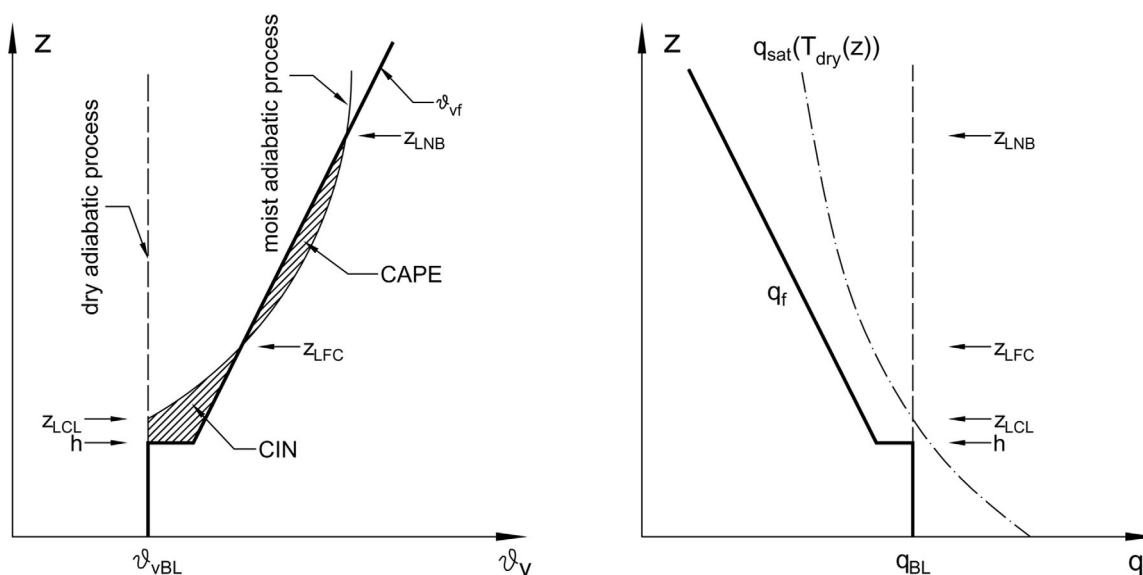


Figure 1. Schematic representation of ABL model and moist convection indicators. Thick solid lines are vertical profiles of virtual potential temperature and specific humidity, thin dash lines are dry adiabatic process, thin solid lines are moist adiabatic process, and thin dash-dot lines are saturation specific humidity at the dry adiabatic temperature (T_{dry}).

convection are controlled by the accumulation of convective available potential energy (CAPE) and convective inhibition (CIN) (as illustrated in Figure 1) up to the time of LCL crossing [Emanuel, 1994; Kirkpatrick *et al.*, 2011]. In particular, it has been shown that to trigger convective rainfall in the midlatitude continental regions, CAPE typically must exceed 400 J kg^{-1} [Battán, 1973; Findell and Eltahir, 2003]. Furthermore, the Storm Prediction Center (SPC) classifies atmospheric instability based on CAPE, as weak ($\text{CAPE} < 1000 \text{ J kg}^{-1}$), moderate ($\text{CAPE} \sim 1000\text{--}2500 \text{ J kg}^{-1}$), strong ($\text{CAPE} \sim 2500\text{--}4000 \text{ J kg}^{-1}$), and extreme ($\text{CAPE} > 4000 \text{ J kg}^{-1}$). Consequentially, CAPE can be used to efficiently interpret the atmospheric instability and diagnose severe thunderstorm environments [Dean *et al.*, 2009].

It is reasonable to conclude that both the time of LCL crossing and the corresponding value of CAPE should be considered as indicators of subsequent moist convection. This changes the model condition from a simple binary crossing/no-crossing of the LCL to the combination of LCL crossing/no-crossing and a CAPE condition of greater/less than certain thresholds (e.g., 400 J kg^{-1}). This simple change creates four possible regimes rather than two. If these regimes were equiprobable, one might expect LCL crossing to be followed by convective precipitation in about half of cases, which is similar to the results of Juang *et al.* [2007b]. Interestingly, as we will demonstrate, the temporal evolution of CAPE, CIN, LCL, and the height of the ABL depend strongly on the combination of soil and atmospheric conditions, unveiling more complex pathways leading to deep convection, which clearly go beyond simple criteria based on the onset of condensation. For example, both wet and dry soils can trigger early moist convection, as demonstrated in Gentine *et al.* [2013], while wet soil usually tends to have a larger magnitude of CAPE as shown later in this study. As a result, convection with early cloud formation under dry soil condition may be too weak to develop into deep convection. Therefore, we contend that special attention should be paid to the joint dynamics of the LCL, CAPE, and CIN and their sensitivities to soil conditions for the understanding of the impacts of land-atmosphere coupling on convective precipitation.

In this study, we embed a simple soil-plant model within a zero-dimensional mixed-layer model of the convective ABL [Garratt, 1992; Porporato, 2009] to simulate the diurnal development of the ABL up to the crossing of the LCL as needed to explore the patterns of LCL crossing time and CAPE. This coupled model captures the essential feedbacks between the land surface and atmosphere within the growing ABL, including the partitioning of surface energy into sensible and latent heat fluxes, the effects of soil and plant water stress in controlling evapotranspiration, as well as entrainment fluxes of moisture and energy from the free atmosphere, and allows for a simultaneous computation of the LCL and CAPE evolution as a function of surface (i.e., soil moisture) and free atmosphere conditions. We tested our results using data from the Central Facility, Southern Great Plains (CF-SGP), where land-atmosphere interactions have been analyzed recently

using the observational data from Atmospheric Radiation Measurement (ARM) Program and Oklahoma Mesonet stations [Chandra et al., 2010; Qian et al., 2013; Ford et al., 2014; Phillips and Klein, 2014]. We only focus on the boundary-layer dynamics before the LCL crossing by using the mixed-layer model, preserving the investigations of the dynamics of cloud-topped boundary layer and preconditions for deep convection for future study, as they involve complicated cloud feedbacks [Lilly, 1968; Stage and Businger, 1981; Zhang and McFarlane, 1995; Stevens, 2006; Zhang and Song, 2009]. The paper is organized as follows: section 2 introduces the ABL model, the soil-plant model, and the convection indicators. Section 3 presents the patterns of LCL crossing times and CAPE dynamics using a parameterization based on atmospheric conditions in CF-SGP. Final conclusions are summarized in section 4. An appendix discusses the pseudoadiabatic processes and the analytical determination of the LCL evolution.

2. Model Description

The essential dynamics of the ABL in the absence of clouds are described using a simple zero-dimensional mixed-layer model, driven by the surface latent and sensible heat flux and by entrainment fluxes of energy and moisture from the free atmosphere. The surface heat flux partitioning is controlled by a soil-plant model, which accounts for the effects of soil moisture stress on vegetation. This coupled soil-plant-ABL model provides the diurnal evolution of the temperature and the humidity in the mixed layer, from which the LCL crossing time and CAPE evolution are computed.

2.1. ABL Model

The simplified zero-dimensional mixed-layer models used in this study were pioneered by Ball [1960], Lilly [1968], Betts [1973], Carson [1973], and Tennekes [1973] in a series of classic studies of simplified models of the ABL. They assumed that (1) the boundary layer is well mixed and thus the virtual potential temperature and specific humidity are constant throughout the ABL, (2) the land surface and the atmosphere are horizontally homogeneous without advection, and (3) the inversion above the ABL is approximated by an instant jump for both temperature and humidity variables [Stull, 1988; Garratt, 1992; Porporato, 2009] (see thick solid lines in Figure 1).

The governing equation for the virtual potential temperature in the boundary layer is given as [Stull, 1988]

$$\rho_a c_p h \frac{d\theta_{vBL}}{dt} = H_v + \rho_a c_p [\theta_{vf}(h) - \theta_{vBL}] \frac{dh}{dt}, \quad (1)$$

where ρ_a is air density, c_p is the specific heat of air, h is the height of ABL, H_v is the surface virtual sensible heat flux [Garratt, 1992; Brutsaert, 1998], and θ_{vBL} and θ_{vf} are the virtual potential temperature within the boundary layer and in the free atmosphere, respectively. The virtual potential temperature is slightly different from the potential temperature due to the lighter density of water vapor and heavier density of liquid water content than that of the dry air [Brutsaert, 1982; Emanuel, 1994],

$$\theta_v = \theta [1 + (R_v/R_d - 1)q - q_l], \quad (2)$$

where R_v and R_d are the gas constant for water vapor and dry air, respectively, q is specific humidity, and q_l is liquid water content, which is zero in this cloud-free ABL.

Similarly, the conservation of water vapor in the boundary layer gives

$$\rho_a h \frac{dq_{BL}}{dt} = E + \rho_a [q_f(h) - q_{BL}] \frac{dh}{dt}, \quad (3)$$

where q_{BL} and q_f are the specific humidity within the boundary layer and in the free atmosphere, respectively, and E is evapotranspiration rate. To close the conservation equations (1) and (3), we use the flux-ratio method, which assumes the buoyancy flux at the inversion is proportional to the surface buoyancy flux [Tennekes, 1973; Garratt, 1992],

$$-\overline{(w'\theta_v')} = \beta \frac{H_v}{\rho_a c_p}, \quad (4)$$

where β is the entrainment ratio which has typical value of 0.2 but may lie between 0.1 and unity [Betts, 1973; Tennekes, 1973; Stull, 1976], and the entrainment buoyancy flux can be linked to the boundary layer growth rate [Garratt, 1992],

$$-(\overline{w'\theta_v'})_h = [\theta_{vf}(h) - \theta_{vBL}] \frac{dh}{dt}. \quad (5)$$

The previous equations allow one to model the evolution of the ABL once the surface fluxes are specified, as described next.

2.2. Soil-Plant Model

The surface sensible (H) and latent (λE) heat fluxes are partitioned from the available energy (Q) [Brutsaert, 2005],

$$Q = H + \lambda E, \quad (6)$$

where λ is the latent heat of water vaporization. The sensible heat flux (H) can be further expressed as [Burke, 1945],

$$H = g_a c_p \rho_a [\theta_s - \theta_{BL}], \quad (7)$$

where c_p is specific heat of air, θ_s and θ_{BL} are the potential temperature at the surface and in the boundary layer, and g_a is the series conductance of leaf boundary layer and atmospheric boundary layer. Likewise, evapotranspiration is modeled as

$$E = \frac{g_a g_s}{g_a + g_s} \rho_a [q_s - q_{BL}], \quad (8)$$

where q_s is the specific humidity at the evaporating surface, and g_s is stomatal conductance, which depends on both plant physiology and environmental conditions [Ball et al., 1987]. This is the link where the soil moisture conditions exert their influence on the land-atmosphere interaction. Specifically, the empirical Jarvis' formulation is used here to model the stomatal conductance [Jarvis, 1976; Daly et al., 2004],

$$g_s = g_{smax} f_Q(Q) f_{\theta_{BL}}(\theta_{BL}) f_{\psi_l}(\psi_l) f_{\delta q}(\delta q), \quad (9)$$

where δq is saturation deficit of specific humidity, defined as

$$\delta q = q_{sat}(\theta_{BL}) - q_{BL}, \quad (10)$$

where the saturation specific humidity q_{sat} is determined by the temperature in the lower level of the boundary layer, which is the same as potential temperature in the mixed layer (θ_{BL}), g_{smax} is the maximum stomatal conductance, ψ_l is the leaf water potential, and f_Q , $f_{\theta_{BL}}$, f_{ψ_l} , and $f_{\delta q}$ are functions of corresponding variables Q , θ_{BL} , ψ_l , and δq , respectively. The water potential gradient from the soil to the leaves drives the water flux into and through the plant,

$$E = g_{srp} (\psi_s - \psi_l), \quad (11)$$

where ψ_s is the soil water potential, which is given by a Brooks-Corey type retention curve [Rodríguez-Iturbe and Porporato, 2005],

$$\psi_s = \bar{\psi}_s s^{-b}, \quad (12)$$

where s is the degree of saturation of soil moisture, b is the exponent of the retention curve, and $\bar{\psi}_s$ is the soil water potential at saturation point [Clapp and Hornberger, 1978]. The soil-root-plant conductance g_{srp} in (11) is the series equivalent of the soil-root conductance and plant conductance,

$$g_{srp} = \frac{L_{AI} g_p g_{sr}}{L_{AI} g_p + g_{sr}}, \quad (13)$$

where L_{AI} is leaf area per unit ground area, g_p is plant conductance in terms of unit leaf area, and g_{sr} is soil-root conductance per unit ground area. The soil-root conductance is modeled as a simplified cylindrical root function [Katul et al., 2003; Rodríguez-Iturbe and Porporato, 2005; Bartlett et al., 2014],

$$g_{sr} = \frac{K \sqrt{R_{AI}} s^{-a}}{\pi g \rho_w Z_r}, \quad (14)$$

where g is gravitational acceleration, ρ_w is water density, K is hydraulic conductivity, a is parameter that attenuates the decrease of g_{sr} due to low hydraulic conductivity under water stress conditions, and R_{AI} is

root area per unit ground area. The hydraulic conductivity and root area index are related to the soil moisture as $K = K_s s^{2b+3}$ [Clapp and Hornberger, 1978], where K_s is the saturated hydraulic conductivity. The plant conductance drops when leaf water potential is low and this decrease is modeled as [Katul et al., 2003]

$$g_p = g_{pmax} \exp \left[- \left(- \frac{\psi_l}{d} \right)^c \right], \tag{15}$$

where the parameters c and d depend on different types vegetation (see detail in Daly et al. [2004]). The above equations model the soil water flow, environmental regulation of stomatal conductance, surface latent and sensible heat fluxes, and atmospheric boundary layer dynamics. This type of simple land surface-ABL system has been extensively tested elsewhere and has been used to analyze the land-atmosphere feedbacks [Daly et al., 2004; Konings et al., 2010; Gentine et al., 2013; Bonetti et al., 2015]. Once soil moisture conditions are specified in (12)–(15) along with boundary-layer conditions in (1) and (3) and radiation forcing in (6), the system can be solved numerically.

2.3. Moist Convection Indicators

The soil-plant-ABL model can be used to simulate the diurnal evolution of temperature and humidity within the mixed layer. By comparing the buoyancy of an adiabatically lifted air parcel with that of the surrounding free atmosphere, suitable indicators of moist convection can thus be derived, as is customary in hydrometeorology [Stull, 1988; Emanuel, 1994; Tsonis, 2002]. When the unsaturated air parcel is adiabatically lifted, the parcel follows a dry adiabatic process (see Appendix A), in which potential temperature and the specific humidity remain constant with height (dashed line in Figure 1), while the parcel temperature decreases according to the dry adiabatic lapse rate. This cooling effect in the dry adiabatic process brings the parcel to saturation at the LCL (see Appendix B and Figure 1). Further adiabatic lifting above the LCL causes an increase in potential temperature due to latent heat release from condensation and the resulting temperature profile follows the so-called moist adiabatic lapse rate, in which equivalent potential temperature is still conserved (see Appendix A and thin solid line in Figure 1).

Due to condensation, the virtual potential temperature will continue to increase as the parcel is lifted higher such that eventually the virtual potential temperature of the air parcel may exceed that of the surrounding air. At this point, termed the level of free convection (LFC), the parcel becomes positively buoyant with respect to the surrounding atmosphere and will continue to rise. Below the LFC, adiabatic lifting results in negative buoyancy and inhibits the convection, while above the LFC the situation is reversed, resulting in positive buoyancy. Further above, the moist adiabat again crosses the surrounding temperature profile (see Figure 1) at the level of neutral buoyancy (LNB), above which the buoyancy with respect to the free atmosphere is again negative. The difference in virtual potential temperature between the adiabatically lifted air parcel and the surrounding atmosphere is a measure of the buoyant force on an air parcel. The total area of positive buoyancy between the LFC and the LNB is thus a measure of buoyant potential energy termed the convective available potential energy (CAPE),

$$CAPE(t) = \int_{z_{LFC}(t)}^{z_{LNB}(t)} g \frac{T_{v,p}(z, t) - T_{v,srd}(z, t)}{T_{v,srd}(z, t)} dz, \tag{16}$$

where $T_{v,p}$ and $T_{v,srd}$ are the virtual temperature of the air parcel and the surrounding air, respectively, and z_{LFC} and z_{LNB} are the height of LFC and LNB, respectively. Note that the CAPE calculated from (16) is based on the temperature of an adiabatically lifted air parcel, which sets the upper limit of the convective energy. In reality, the air parcel cannot utilize all the CAPE due to the entrainment of dry and warm air [Zhang and McFarlane, 1991; Zhang, 2009]. In this study, only the conventional definition of CAPE is used to track the moist convection. Similarly, the total negative buoyancy below the LFC will restrain the rising air parcel and is defined as convective inhibition (CIN),

$$CIN(t) = - \int_{z_0}^{z_{LFC}(t)} g \frac{T_{v,p}(z, t) - T_{v,srd}(z, t)}{T_{v,srd}(z, t)} dz, \tag{17}$$

where z_0 is the height at the earth surface.

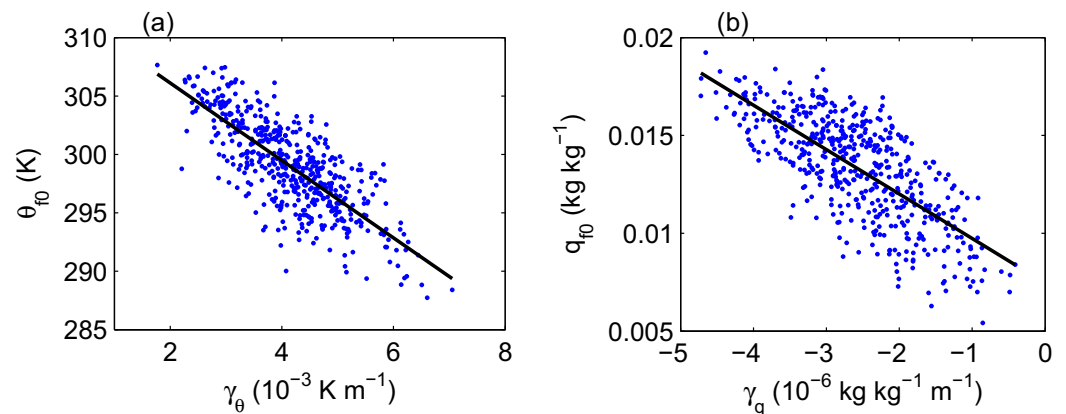


Figure 2. Scatter plots of (a) morning potential temperature surface value θ_{f0} versus lapse rate γ_θ and (b) morning humidity surface value q_{f0} versus profile slope γ_q .

3. Results

The ABL model of section 2 can be numerically solved to obtain the dynamics of LCL, CAPE, and CIN (as described in Appendices A and B and section 2). This model is parameterized and analyzed with reference to a well-defined field experiment described next.

3.1. Study Site

To analyze the land-atmosphere coupling and its effects on moist convection, we focus on summer conditions observed in the Central Facility, Southern Great Plains (CF-SGP), which is characterized by strong land-atmosphere coupling in the warm seasons [Koster *et al.*, 2004] but may also have strong synoptic forcing such as low-level jet influence. Recently, the area has been extensively studied using the observational data from ARM Program and Oklahoma Mesonet stations [Chandra *et al.*, 2010; Qian *et al.*, 2013; Ford *et al.*, 2014; Phillips and Klein, 2014].

Radiosonde data from the ARM program (<http://www.arm.gov/>) in the summer early morning (0530 local time) are used to analyze the atmospheric conditions in CF-SGP. The virtual potential temperature and specific humidity tend to be linearly related to the altitude and therefore may be approximated as linear functions (note that this assumption can be easily relaxed),

$$\theta_{vf}(z) = \gamma_{\theta_v} z + \theta_{vf0}, \quad (18)$$

and

$$q_f(z) = \gamma_q z + q_{f0}. \quad (19)$$

where γ_{θ_v} and γ_q are the slopes of θ_v and q , respectively, and θ_{vf0} and q_{f0} are the surface values of θ_v and q , respectively. These slopes and surface values for CF-SGP, as seen in Figure 2, are negatively correlated, indicating that less stable free atmosphere conditions tend to correspond to a warmer land surface, while wetter air in the lower atmosphere is associated with rapid decreases in upper atmosphere moisture. Similar correlations were also observed in other regions [Konings *et al.*, 2010]. Based on these observations, the surface values (θ_{vf0} , q_{f0}) are modeled as linear functions of the slopes (γ_{θ_v} , γ_q) to reduce the number of parameters describing the states of the free atmosphere.

Surface heat fluxes in CF-SGP were measured at 30 min intervals with an Energy Balance Bowen Ratio (EBBR) Station from ARM program. The available energy shows a daily progression well approximated by a parabolic function with peak value $Q_{\max} = 490 \text{ W m}^{-2}$ at midday ($t = 6 \text{ h}$) and zero value at $t = 0 \text{ h}$ and $t = 12 \text{ h}$ (thin solid curves in Figure 3b). The soil and vegetation parameters are the same as in Daly *et al.* [2004], representing the typical C3 plants and silt loam soil at CF-SGP.

3.2. Diurnal Evolution

We first show the diurnal evolution of surface energy partitioning with typical free atmosphere conditions parameterized on 18 July 2009 (see Table 1), under different soil moisture conditions from well watered to a

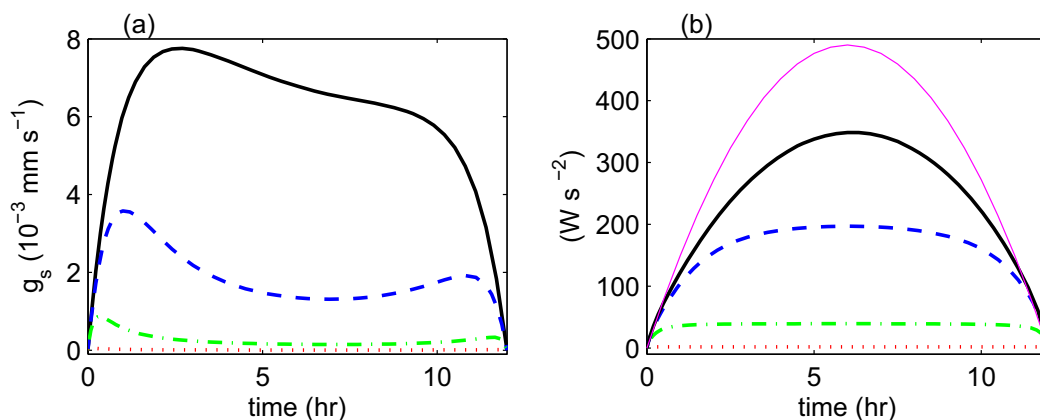


Figure 3. (a) Stomatal conductance and (b) latent heat flux for different soil moisture conditions $s = 0.45$ (thick solid line), $s = 0.38$ (thick dash line), $s = 0.32$ (thick dash-dotted line), and $s = 0.25$ (thick dotted line). The thin solid line in Figure 3b is the total available energy Q . The soil and vegetation parameters are the same as in *Daly et al.* [2004], and the atmospheric parameters are in Table 1.

condition near the wilting point. The plants are assumed to begin closing stomata in response to water stress when soil moisture is below $s^* = 0.45$, and reach complete closure when soil moisture is below the wilting point $s_w = 0.25$. As can be seen in Figure 3, the stomatal conductance generally follows the variation of radiation under well-watered condition, while it decreases sharply in midday in conditions of water stress. The transpiration shows a related pattern with a flattening due to stomatal closure [*Daly et al.*, 2004].

The soil moisture control on evapotranspiration via stomatal conductance affects the energy partitioning and thus the boundary-layer dynamics [*Jarvis*, 1976; *McNaughton and Spriggs*, 1986; *Daly et al.*, 2004]. Figure 4 shows the diurnal evolution of ABL, LCL, LNB, and LFC under various soil conditions. During the day, both ABL and LCL increase and end up crossing in the afternoon. On the contrary, LFC decreases while the LNB increases so that the gap between each other gradually widens. Under drier soil condition, more sensible heat flux is added into the ABL, which thus grows faster and crosses the LCL earlier. However, the distance between the LFC and LNB increases slower than under wetter soil conditions. Due to the continuous supply of water from the surface, the LCL stays low causing a faster increase in CAPE (Figure 5). This soil moisture control on ABL and LCL is consistent with the observation in SGP [*Phillips and Klein*, 2014]. Here the specific atmosphere could be classified as “dry soil advantage” atmosphere in terms of LCL crossing, as an earlier crossing is possible under dry soil condition. Similar atmospheric conditions are also identified by tracking the relative humidity at the top of the boundary layer in some studies [*Ek and Holtslag*, 2004; *Westra et al.*, 2012; *Gentine et al.*, 2013]. However, this atmosphere could also be classified as “wet soil advantage” atmosphere in terms of CAPE as the simulations show higher CAPE under wet soil condition. This contrasting pattern will be further explored under more comprehensive atmospheric conditions.

Clouds may be assumed to develop as soon as the ABL crosses the LCL. At this time, the state of ABL is critical for the following development of potential deep convection. For example, an early LCL crossing ensures that solar radiation is still available to sustain the continued convection. By investigating the timing of the initiation of moist convection, *Gentine et al.* [2013] found that both wet soil and dry soil may be conducive to early moist convection when changing the atmospheric parameters, meaning that the atmospheric conditions can determine whether the soil moisture-rainfall feedback is positive or negative.

Other than the timing of moist convection, the amount of accumulated convective potential energy as CAPE at that time determines whether the ABL is well prepared for the following development of deep convection. As a general rule of thumb, CAPE larger

Table 1. Atmospheric Parameters in the Early Morning on 18 July 2009 at CF-SGP

Variables	Value	Unit
γ_{div}	0.0033	$K m^{-1}$
θ_{vfo}	298	K
γ_q	-2.1×10^{-6}	$kg kg^{-1} m^{-1}$
q_{fo}	0.011	$kg kg^{-1}$
Q_{max}	490	$W m^{-2}$

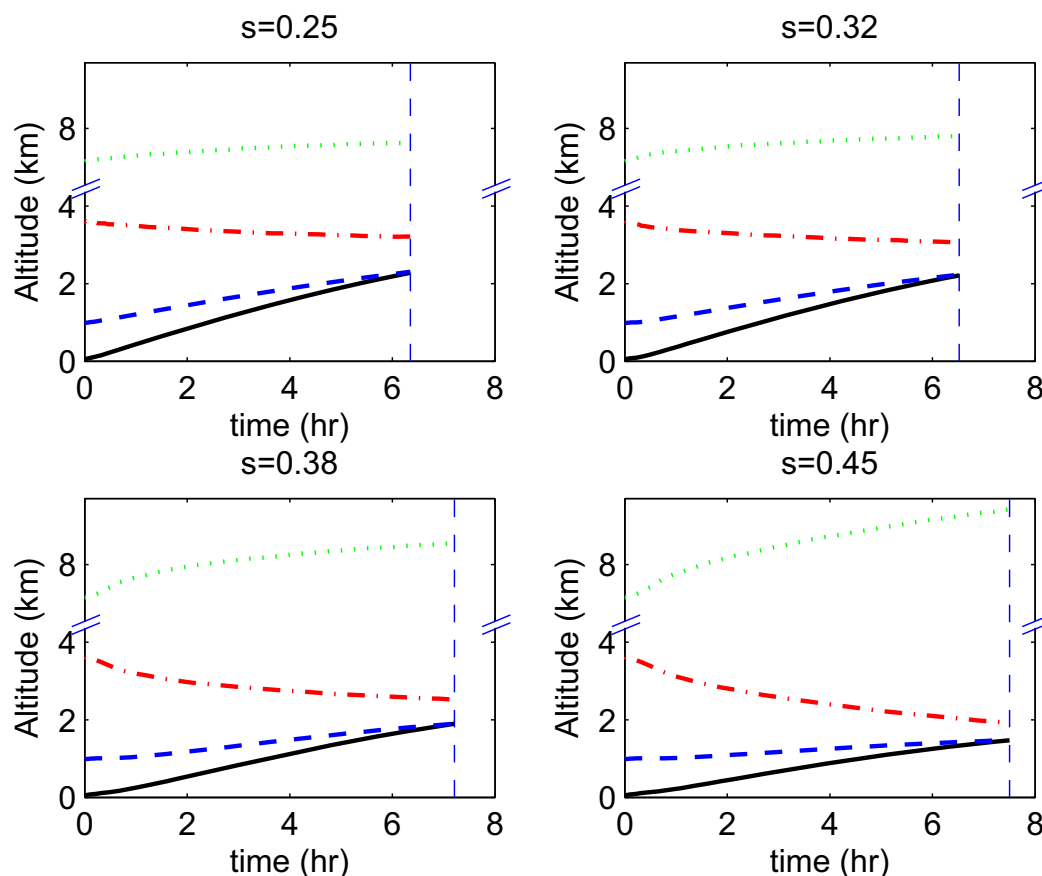


Figure 4. ABL height (black solid), LCL (blue dash), LFC (red dash-dot), and LNB (green dot) evolution under different soil moisture conditions. The vertical thin dash lines mark the LCL crossing time. Note that the y axis has been cut between 4 and 6 to facilitate comparison of the evolution of the different altitudes. Parameters are the same as in Figure 3.

than 400 J kg^{-1} is required [Findell and Eltahir, 2003] and this empirical threshold will be used here as a criterion for deep convection along with the LCL crossing.

3.3. Soil Moisture and Atmospheric Controls on Moist Convection: Classification of Different Regimes

The previous section referred only to one specified atmospheric condition. In this section, we explore the effect of free atmospheric conditions. To constrain the parameter space, we employ the linear relationship between slope and surface values for the free atmospheric profiles presented in Figure 2. With this linear relationship, a smaller γ_{θ_v} means that the free atmosphere is less stable and hotter near the earth surface, while a smaller γ_q means that the free atmosphere is wetter in the lower altitude but drier at higher elevation in terms of specific humidity. Exploring these parameters allows us to account for a comprehensive range of atmospheric conditions through the analysis of the parameters γ_q and γ_{θ_v} under different soil moisture conditions.

Regimes for the conditions of the LCL crossing and the CAPE at the time of the crossing (or at the end of the day if there is no crossing) are presented in Figures 6 and 7 and are summarized in Table 2. When atmospheric conditions are within regime I, the CAPE is larger than 400 J kg^{-1} at the end of the day but the ABL does not cross the LCL. Within regime II, the CAPE is too low at the end of the day while ABL still does not cross the LCL. In regime III, ABL crosses the LCL but the CAPE is too low ($<400 \text{ J kg}^{-1}$) at the crossing time. Only when the atmospheric conditions are within regime IV, is deep convection likely to be triggered, since the CAPE is large enough when the ABL crosses the LCL.

The analysis of these four regimes as a function of free atmospheric parameters for different soil moisture conditions is presented in Figure 6. In general, the regimes I, II, III, and IV map onto four quadrants, corresponding to near neutral-and-dry, stable-and-dry, stable-and-moist, and near neutral-and-moist atmosphere. Particularly, in the bottom right of regime IV (the lower atmosphere is relatively more stable and

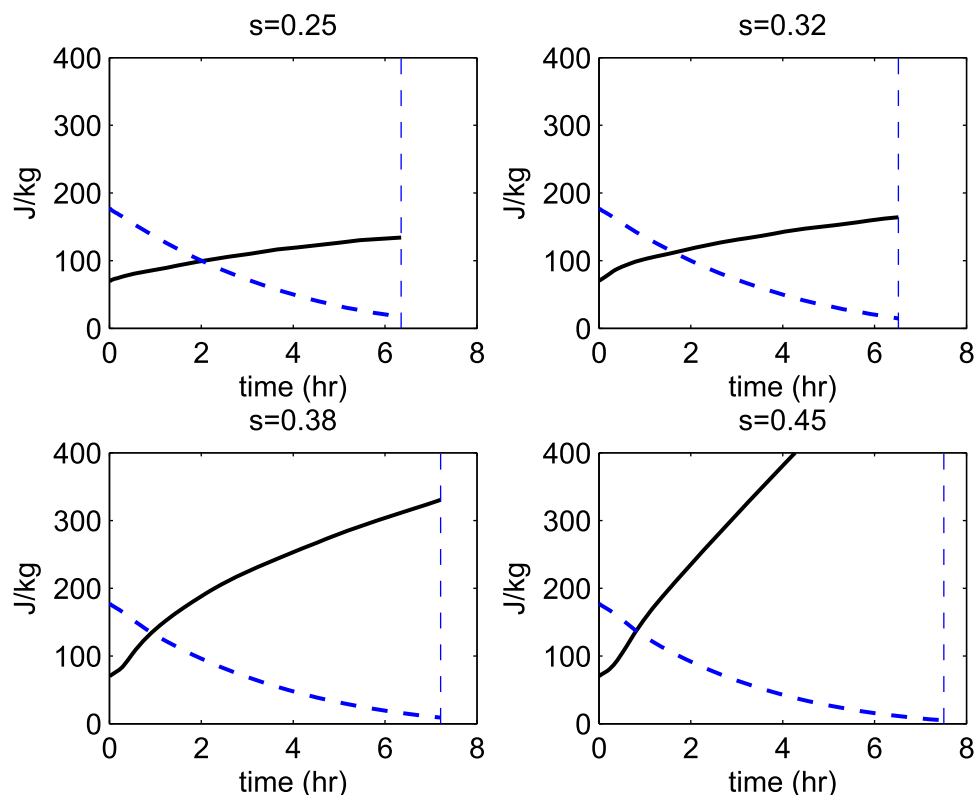


Figure 5. CAPE (black solid) and CIN (blue dash) evolution under different soil moisture conditions. The vertical thin dash lines mark the LCL crossing time. Parameters are the same as in Figure 3.

wetter), the ABL grows slowly but efficiently accumulates moisture, thus facilitating the LCL crossing. In the top left of regime IV (the lower atmosphere is relatively less stable and drier), the moist convection still can be triggered in the dry soil condition, under which more available energy is partitioned into sensible heat flux which then accelerates the growth of ABL to reach the LCL. This regime is close to the atmospheric conditions analyzed in section 3.2 and also has been identified as “dry soil advantage” atmosphere in some other studies [Ek and Holtslag, 2004; Westra et al., 2012; Gentine et al., 2013].

The values of CAPE at the time of LCL crossing corresponding to Figure 6 are presented in Figure 7. As can be seen, the CAPE and the LCL crossing time show different patterns with respect to atmospheric conditions. While the ABL can cross the LCL earlier under either wetter or drier soil (Figure 6), the CAPE seems always larger under wetter soil conditions (Figure 7). Besides the soil conditions, the free atmosphere can also influence the intensity of convection. A less stable atmosphere tends to provide more positive buoyancy to the air parcel and moist atmosphere could decrease the LCL [Stull, 1988; Emanuel, 1994; Tsonis, 2002]. This is reflected in Figure 6, where CAPE becomes larger for smaller γ_q and γ_{θ_v} . The empirical CAPE threshold, defining the boundaries between regimes I and II and between regimes III and IV, is used to estimate the transition to shallow or to deep convection. A slight change of this threshold does not qualitatively change the general location of regimes I–IV. For example, if the threshold decreases to 300 J kg^{-1} , the boundaries between regimes I and II and between regimes III and IV will follow the CAPE contours and slightly move to the right, leading to a corresponding expansion of regimes I and IV and a contraction of regimes II and III. If the threshold is increasing to 500 J kg^{-1} , the boundaries will slightly move to the left and have opposite effects on the area of each regime.

Due to these contrasting patterns between the CAPE and the LCL crossing, we will analyze their joint dynamics next to understand the possible conditions that favor convective precipitation.

3.4. Soil Moisture Sensitivity to the Moist Convection

As shown in the previous sections, earlier LCL crossings are not necessarily accompanied by larger CAPE and in general both of these two indicators should be taken into consideration. Given their possible

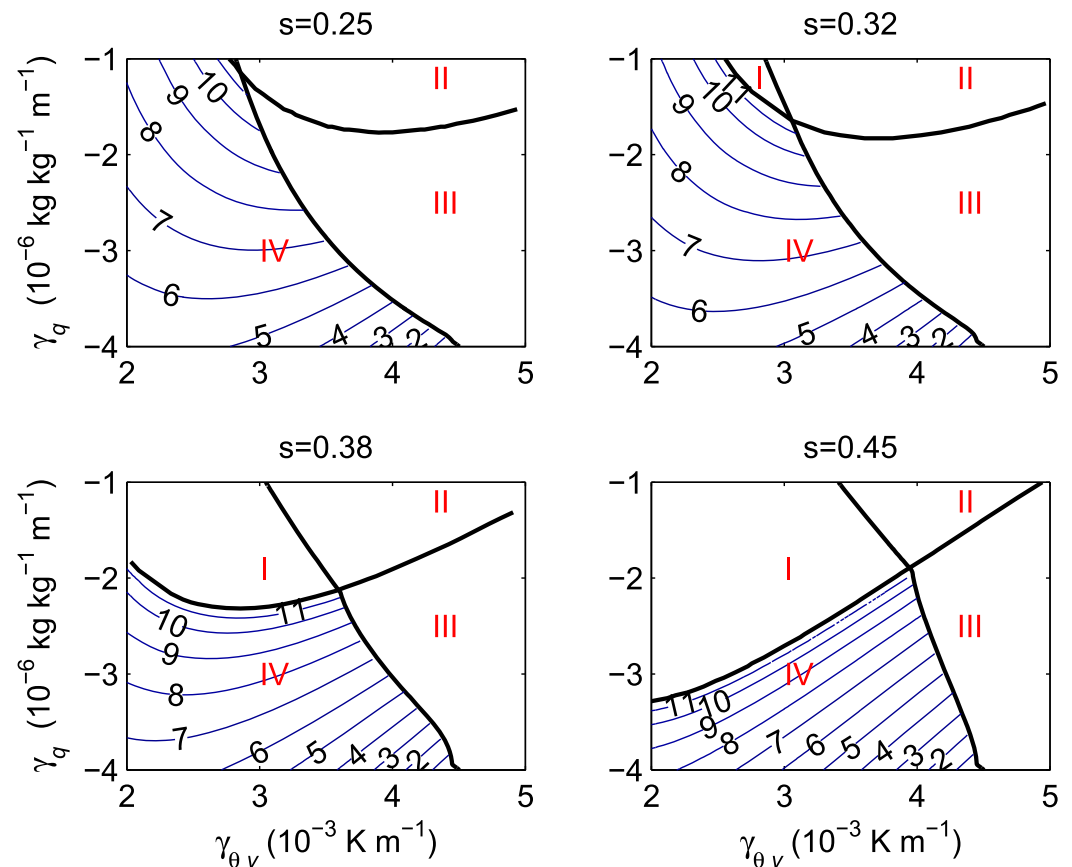


Figure 6. LCL crossing time under different soil moisture and atmospheric conditions. Labeled contour lines represent the hour after sunrise that LCL crossing occurs. No crossing occurs in regions I–III. Classification of regime I–IV is described in Table 2.

contrasting tendencies, one specified free atmosphere condition may have the strongest convection when the soil moisture value is such that it corresponds to the highest CAPE while still allows the ABL to cross the LCL during the daytime. We will indicate this soil moisture corresponding to maximum convection as s_{\max} and study its behavior as a function of free atmospheric conditions. Note that although the overall influence of soil moisture on rainfall frequency is more significant than the influence on rainfall intensity over a long period of time [D’Odorico and Porporato, 2004; Findell et al., 2011; Yin et al., 2014], for specific atmospheric conditions, soil moisture can influence the states of the atmosphere such as low-level humidity, which then could determine both the occurrence and intensity of the rainfall event [Bretherton et al., 2004; Neelin et al., 2009].

Figure 8 shows the LCL crossing time (solid lines) and the corresponding CAPE (dash lines) as a function of soil moisture under four types of atmospheric conditions. For example, in Figure 8a, the ABL can cross LCL only when soil is dry ($s \leq 0.34$), while CAPE increases as the soil becomes wetter, indicating $s_{\max} = 0.34$ could potentially trigger the strongest moist convection. Figure 8b shows a similar pattern for an intermediate value of s_{\max} . The example conditions of Figures 8c and 8d show another type of atmosphere under which the ABL always crosses LCL and CAPE increases as the soil become wetter, suggesting a scenario where the wettest soil could trigger the strongest deep convection ($s_{\max} = 0.5$).

The soil moisture corresponding to the maximum convection (s_{\max}) could be further used to classify the sensitivity of moist convection to soil moisture. If s_{\max} is small (as in Figure 8a), the specified atmosphere can be classified as a “dry soil advantage” atmosphere. If s_{\max} is large (as in Figures 8c and 8d), the atmosphere can be classified as a “wet soil advantage” atmosphere. The intermediate case of Figure 8b can be classified as a “transitional” atmosphere. Other than comparing the simulated rainfall occurrence only under the extreme wet and dry soil moisture cases [Findell and Eltahir, 2003], this s_{\max} tests the whole range of soil moisture to provide a more accurate soil moisture condition corresponding to maximum convection. This

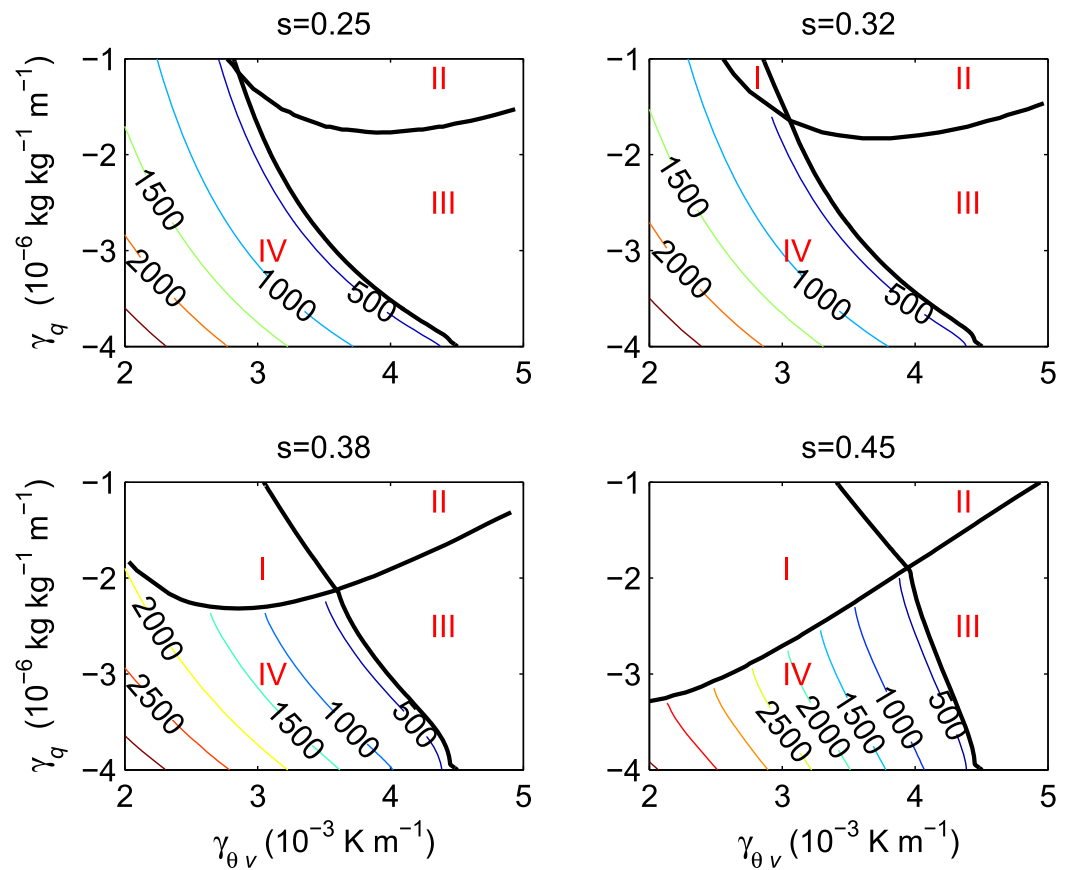


Figure 7. CAPE levels at the LCL crossing time for four different soil moisture conditions as a function of free atmospheric conditions. The thick solid lines divide the atmospheric conditions into four regimes I–IV based on the LCL crossing and the CAPE, which are explained in Table 1. Contours in regime IV represent the CAPE at the time of LCL crossing in units of J kg^{-1} . Note that the CAPE contours do not follow the crossing time contours of Figure 6.

accurate s_{max} involves a trade-off between LCL crossing and the intensity of the convection and helps identifying the nonlinearity of the feedbacks in the land-atmosphere interactions.

Based on the analysis of s_{max} , the atmospheric conditions can be divided into four different zones as shown in Figure 9 and summarized in Table 3: in zone A, the ABL cannot cross LCL under any soil moisture condition; in zone B, the ABL can cross LCL under any soil moisture condition but the CAPE at the time of crossing is lower than 400 J kg^{-1} ; in zone B', the ABL can cross LCL under certain soil moisture condition but CAPE at the time of crossing is low; only in zone C, can the ABL cross LCL in the daytime with a maximum CAPE larger than 400 J kg^{-1} , so that s_{max} can be found. Unlike the classification of atmosphere regimes in section 3.3 (Table 2), which is based on one specified soil moisture condition, the classification of atmospheric zones in this section (Table 3) considers the whole range of soil moisture to identify the state corresponding to the maximum convection (s_{max}).

Figure 9 also marks the four example atmospheric conditions of Figure 8 as the star, circle, cross, and plus. As can be seen, when the near neutral free atmosphere is dry near the surface but moist in the higher altitude (large γ_q and small γ_{θ_v} , around the star mark), s_{max} is small and a negative feedback can be identified between the soil moisture and the moist convection. When the lower atmosphere is moist (small γ_q , around the cross and the plus), s_{max} is large and a positive feedback can be identified. When the lower atmosphere is near neutral and

Table 2. Regime Classification of Atmospheric Conditions as in Figures 6 and 7 Based On the LCL Crossing and the CAPE at the Time of the Crossing (or End of the Day if There Is No Crossing)

Regime	LCL Crossing	CAPE (J kg^{-1})
I	No	>400
II	No	<400
III	Yes	<400
IV	Yes	>400

altitude (large γ_q and small γ_{θ_v} , around the star mark), s_{max} is small and a negative feedback can be identified between the soil moisture and the moist convection. When the lower atmosphere is moist (small γ_q , around the cross and the plus), s_{max} is large and a positive feedback can be identified. When the lower atmosphere is near neutral and

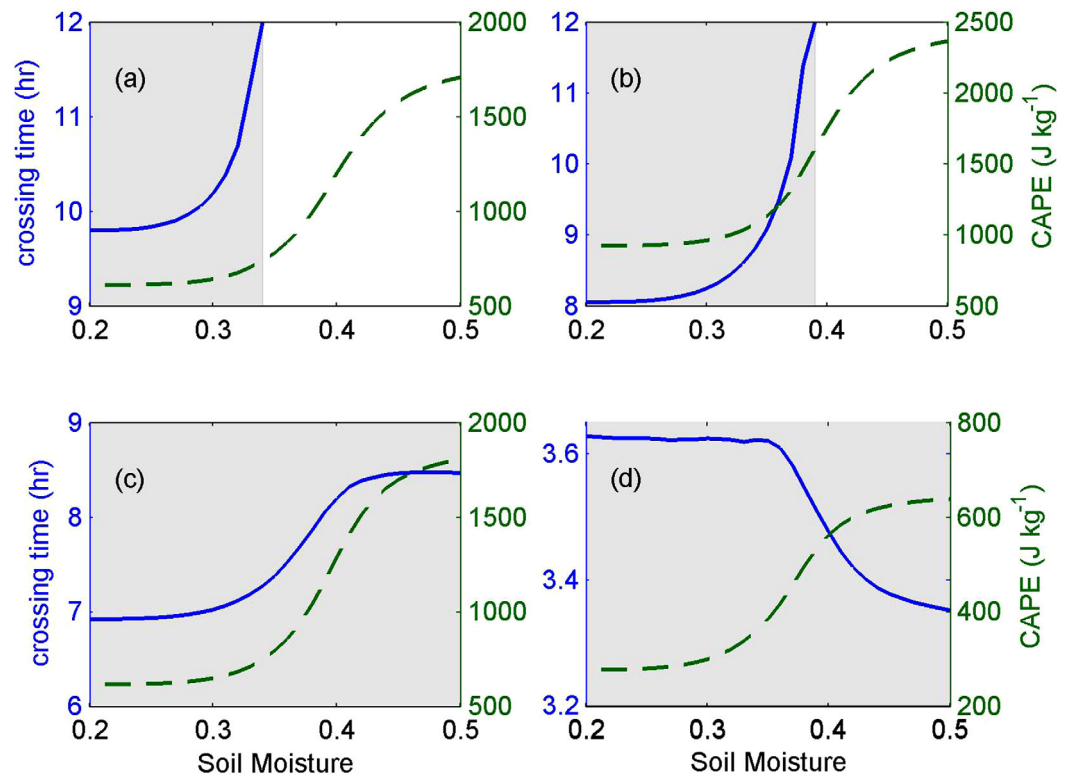


Figure 8. LCL crossing time (solid lines) and CAPE (dash lines) as a function of soil moisture for four typical atmosphere conditions: (a) $\gamma_{\theta v} = 2.7 \times 10^{-3} \text{ K m}^{-1}$, $\gamma_q = -1.5 \times 10^{-6} \text{ kg kg}^{-1} \text{ m}^{-1}$; (b) $\gamma_{\theta v} = 2.7 \times 10^{-3} \text{ K m}^{-1}$, $\gamma_q = -2.4 \times 10^{-6} \text{ kg kg}^{-1} \text{ m}^{-1}$; (c) $\gamma_{\theta v} = 3.3 \times 10^{-3} \text{ K m}^{-1}$, $\gamma_q = -3 \times 10^{-6} \text{ kg kg}^{-1} \text{ m}^{-1}$; (d) $\gamma_{\theta v} = 4 \times 10^{-3} \text{ K m}^{-1}$, $\gamma_q = -3.5 \times 10^{-6} \text{ kg kg}^{-1} \text{ m}^{-1}$; these four cases are also represented in Figure 9 as star, circle, cross, and plus. The shaded area is the region where ABL is able to reach the LCL at the daytime.

moist (small $\gamma_{\theta v}$ and small γ_q , around the circle mark), s_{\max} is between dry and wet, showing the transition from positive to negative feedback. In general, this coupled soil-plant-ABL model demonstrates that the soil moisture feedbacks to moist convection are nonlinear and dependent on the free atmospheric conditions. The feedbacks would become even more complicated when considering large-scale circulation as have

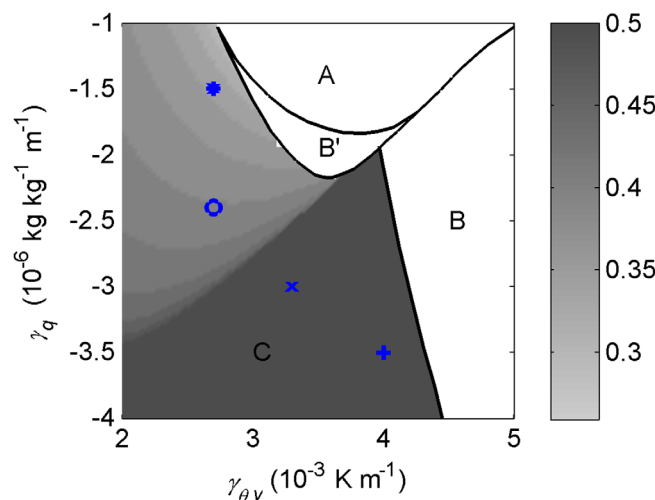


Figure 9. Soil moisture corresponding to the maximum convection (s_{\max}) under various atmospheric conditions. The star, circle, cross, and plus represent four corresponding atmosphere conditions in Figures 8a, 8b, 8c, and 8d. The thick solid lines divide the atmospheric conditions into four different zones A, B', B, and C, which are explained in Table 3.

been observed in many recent studies [Findell et al., 2011; Taylor et al., 2012; Guillod et al., 2015].

In the analysis above, the use of linear state profiles reduces the number of parameters to capture the essential features of atmospheric conditions. This also allows us to visualize the classification of free atmosphere and soil moisture regimes and thus illustrate the effects of land and atmospheric controls on the moist convection. In practice, the mixed-layer models and the classification methods can be directly applied to observed radiosonde data. To demonstrate this, we used observed early morning sounding profiles and surface heat fluxes in CF-SGP from the summer of 2002–2009 to analyze the soil moisture sensitivity to moist convection (days with

Table 3. Atmospheric Zones as in Figure 9 Based On the LCL Crossing, and Maximum CAPE at the Time of the Crossing

Zone	LCL Crossing	Maximum CAPE ($J\ kg^{-1}$)
A	No, for any soil moisture	
B	Yes, for any soil moisture	<400
B'	Yes, for a range of soil moisture	<400
C	Yes, for a range of soil moisture	>400

missing data were excluded from this analysis). From these 365 days of free atmosphere profiles, 168 days are classified into zone A, 13 days into zone B, 38 days into zone B', and 146 days into zone C. The distribution of s_{max} for these 146 free atmosphere profiles in zone C is presented in Figure 10. It shows that soil moisture conditions

from wet to dry can possibly trigger the strongest convection, indicating that all three types of atmospheric conditions (i.e., "positive soil advantage," "transitional," and "negative soil advantage" atmospheric conditions) exist in CF-SGP. This analysis is consistent with the study of *Findell and Eltahir [2003]*, which compared the modeled convective rainfall under two extreme soil moisture conditions and concluded Oklahoma is in the transitional feedback region.

3.5. Moist Convection Under Other Land Surface and Atmospheric Conditions

The regime classification discussed before refers to clear sky conditions and is limited to the regression relationships of temperature and humidity profiles as in Figure 2. Other effects may induce some variations in terms of the LCL crossing and CAPE in different conditions. For example, when early morning clouds are above the newly developed boundary layer, part of the solar radiation can be reflected and absorbed by the liquid water in the cloud. The reduction of surface radiation could not only delay the initiation of moist convection but also reduce the intensity of convection. As a result, the area of the atmospheric zone C, representing the possible deep convection zone, will shrink, indicating more difficulty to trigger deep convection.

If the atmospheric conditions are warmer than usual (e.g., increase θ_{f0}) but with the same specific humidity profiles, the atmosphere will have a higher water vapor saturation capacity so that the LCL is higher and CAPE is lower than usual. For these reasons, it is more difficult to trigger deep convection under the warmer-than-usual atmosphere. Similarly, if the atmospheric conditions are wetter than usual (e.g., increase q_{f0}) but with the same temperature profiles, the atmosphere needs less water vapor to become saturated so that the LCL is lower and CAPE can be higher than usual. The wetter-than-usual atmosphere more easily triggers deep and strong convection.

Regarding the land surface conditions, the foregoing development assumes a typical C3 plant cover. It could be interesting to analyze the impact of different photosynthetic pathways [*Lüttge, 2000; Daly et al., 2004; Vico and Porporato, 2008; Borland et al., 2009; Hartzell et al., 2015*] and land cover types [*Pitman, 2003; Pielke et al., 2011*], in general, on atmospheric convection. For example, C4 plants are more sensitive to water stress and may have less transpiration in semiarid regions [*Vico and Porporato, 2008*], thus partitioning more sensible heat flux to accelerate the boundary-layer growth.

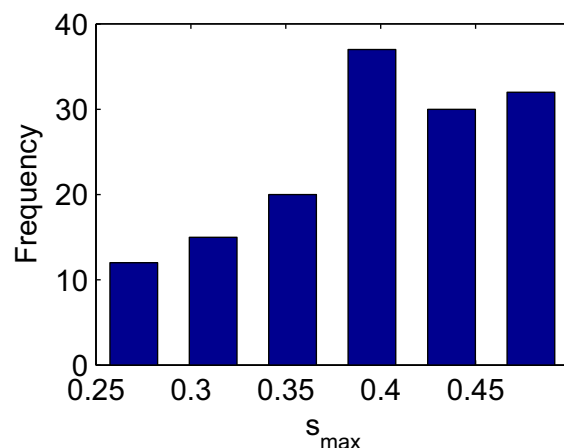


Figure 10. Distribution of soil moisture corresponding to the maximum convection (s_{max}) calculated from observational data in Central Facility, Southern Great Plains.

4. Conclusions

In this study, we embedded a soil-plant system within a mixed-layer model to study the possible conditions that could lead to deep convection with consideration of both the initiation of moist convection (LCL crossing) and the convective energy (CAPE threshold). Based on the free atmosphere conditions in Central Facility, Southern Great Plains, we found that a dry atmosphere tends to suppress moist convection and stable atmosphere tends to have less convective energy. Moist convection can be triggered earlier when the atmosphere is more

stable and wetter, which allows the ABL to grow slowly but efficiently accumulate moisture, thus facilitating the LCL crossing. CAPE is found to be always larger over the wetter surface, which provides abundant moisture content to lower the LCL and increase the buoyancy of the lifted air parcel.

By combining a CAPE threshold condition to the traditional binary criterion of crossing/no-crossing of the LCL, our analysis defines four different atmospheric regimes and maps their existence as a function of the boundary conditions (i.e., soil moisture properties, plant, and free atmosphere parameters) to illustrate the complicated dependence of boundary-layer dynamics and deep convection on soil moisture and atmospheric conditions. We also investigated the soil moisture corresponding to the maximum potential convection (i.e., the largest CAPE at time of LCL crossing), which provides a criterion to identify which soil moisture state favors the strongest convection. While the CAPE here is close to the Convective Triggering Potential of *Findell and Eltahir* [2003], our approach considers the whole range of soil moisture when quantifying the maximum potential convection. By adding CAPE to the previous single criterion of LCL crossing [e.g., *Juang et al.*, 2007a; *Siqueira et al.*, 2009; *Gentine et al.*, 2013], the categorization of atmospheric conditions becomes more precise regarding the so-called dry or wet soil advantage for triggering convection. For example, while previous work identified the dry soil advantage only in terms of LCL crossing (e.g., Figure 8c), from our analysis it becomes clear that these atmospheric conditions should instead be identified as wet soil advantage when considering also that CAPE is always higher under wet soil conditions.

Finally, it should be kept in mind that this study has been focused on the development of the ABL and CAPE only up to the LCL crossing. The emergence of convective cloud cover after the LCL crossing will significantly influence the entrainment flux by redistributing the radiation and by evaporating liquid water in the cloud. It will be interesting in future work to go beyond these simplifications, especially to include the dynamics of the cloud-topped boundary layer to link the CAPE at LCL crossing to the actual onset and development of free convection. With longer time scales in mind, the result of this work may be used to interpret simplified representations of soil moisture-rainfall feedback parameterization in stochastic soil moisture models [*D’Odorico and Porporato*, 2004; *Porporato and D’Odorico*, 2004; *Yin et al.*, 2014].

Appendix A: Thermodynamic Background and Definition of Pseudoadiabatic Processes

Since adiabatic lifting includes no heat exchange between the air parcel and the surrounding atmosphere, the first law of thermodynamics implies that the work done by changing the specific volume of air parcel ($d\alpha$) against the surrounding pressure (P) is completely going into internal energy ($c_v dT$),

$$c_v dT = -Pd\alpha, \tag{A1}$$

where c_v is the specific heat at constant volume and dT is the change of the temperature. Using Mayer’s relation between specific heats

$$c_p - c_v = R, \tag{A2}$$

where c_p is specific heat at constant pressure and the differential form of the ideal gas law

$$RdT = d(\alpha P) = Pd\alpha + \alpha dP, \tag{A3}$$

allows one to write for the dry adiabat,

$$c_p dT = \alpha dP = \frac{1}{\rho_a} dP, \tag{A4}$$

where $c_p dT$ is the change of enthalpy for the perfect gas.

In a moist pseudoadiabatic process, where the heat capacity of liquid water is neglected, the latent heat release from condensed liquid water content (dq_L) provides extra enthalpy for the air parcel, so that

$$c_p dT = \frac{1}{\rho_a} dP + \lambda dq_L. \tag{A5}$$

Since condensation takes place at the saturation curve, dq_L can be expressed as

$$dq_L = -dq_{sat}(T, P). \tag{A6}$$

Using the ideal gas law and substituting (A6) into (A5), one obtains an ordinary differential equation for the moist pseudoadiabatic process,

$$c_p dT = \frac{RT}{P} dP - \lambda dq_{sat}(T, P). \tag{A7}$$

By approximating the gas constant of the air parcel using that of dry air,

$$q_{sat}(T, P) = \frac{R e_{sat}(T)}{R_v P} \approx \varepsilon \frac{e_{sat}(T)}{P}, \tag{A8}$$

where ε is the ratio of gas constant of dry air to that of water vapor, e_{sat} is saturation water vapor pressure, which is governed by the parcel temperature following the relationship described in the Clausius-Clapeyron equation,

$$\frac{de_{sat}}{dT} = \frac{\lambda e_{sat}}{R_v T^2}. \tag{A9}$$

Differentiating the saturation specific humidity in (A7) with the approximation (A8) and the Clausius-Clapeyron equation (A9), one can find the temperature change with respect to pressure [Emanuel, 1994; Tsonis, 2002],

$$\frac{dT}{dP} = \frac{1}{P} \frac{RT + \lambda q_s}{c_p + \frac{\lambda^2 q_s}{R_v T^2}}. \tag{A10}$$

In practice, the adiabatic lapse rate is often expressed as the rate of temperature change with increase in altitude. To obtain these types of lapse rates, one may assume that the surrounding atmosphere is in hydrostatic equilibrium, in which case

$$\frac{dP}{dz} = - \frac{Pg}{RT_{srd}}, \tag{A11}$$

where T_{srd} is the temperature of the surrounding air. With this, assuming the surrounding air and the parcel air have the same temperature (i.e., $T = T_{srd}$) and substituting (A11) into (A4) yields another form of dry adiabatic lapse rate, i.e.,

$$\Gamma_{dry} = \frac{dT}{dz} = - \frac{T}{T_{srd}} \frac{g}{c_p} \approx - \frac{g}{c_p}, \tag{A12}$$

while substituting (A11) into (A10) yields another form of moist pseudoadiabatic lapse rate,

$$\Gamma_{moist} = \frac{dT}{dz} = - \frac{g}{c_p} \frac{RT + \lambda q_s}{1 + \frac{\lambda^2 q_s}{c_p R_v T^2}} \frac{1}{RT_{srd}} \approx - \frac{g}{c_p} \frac{1 + \frac{\lambda q_s}{RT}}{1 + \frac{\lambda^2 q_s}{c_p R_v T^2}}. \tag{A13}$$

It is worth mentioning that the approximation in equations (A12) and (A13) may become inaccurate due to the assumption of $T_{srd} = T$, especially when the surrounding air and parcel air have significant temperature difference (e.g., atmospheric condition with large CAPE).

Appendix B: Analytical Determination of the LCL Evolution

During a dry adiabatic lifting process, no water vapor is condensed and thus the specific humidity of the air parcel remains constant. At the lifting condensation level (LCL), the air parcel just becomes saturated but its specific humidity still equals the initial value (q_0),

$$q_{LCL} = \varepsilon \frac{e_s(T_{LCL}(P_{LCL}))}{P_{LCL}} = q_0, \tag{B1}$$

where $e_s(\cdot)$, the saturation water vapor pressure as a function of temperature, can be derived from the Clausius-Clapeyron equation. Assuming constant latent heat of vaporization λ in (A9), the Clausius-Clapeyron equation can be written in the integrated form as

$$e_{sat}(T) = e_{sat}(T_{ref}) \exp \left[\frac{\lambda}{R} \left(\frac{1}{T_{ref}} - \frac{1}{T} \right) \right], \quad (B2)$$

where T_{ref} and $e_{sat}(T_{ref})$ are the reference temperature and the saturation vapor pressure at the reference temperature, respectively. Since the air parcel follows the dry adiabatic process from near-surface initial temperature T_0 , the temperature at LCL $T_{LCL}(P_{LCL})$ can be found by integrating equation (A4),

$$T_{LCL} = T_0 \left(\frac{P_{LCL}}{P_0} \right)^{R/c_p}. \quad (B3)$$

Finally, the pressure at the LCL can be analytically solved from equations (B1–B3), yielding the closed form

$$P_{LCL} = \frac{(\lambda R)^{c_p/R}}{\left\{ -c_p R_V T_0 W \left[-\frac{q_0 \lambda R}{e_{sat}(T_{ref}) c_p R_V T_0} \exp \left(-\frac{\lambda R}{c_p R_V T_{ref}} \right) P_0^{R/c_p} \right] \right\}^{c_p/R}} P_0, \quad (B4)$$

where $W[\cdot]$ is the Lambert W function [Corless *et al.*, 1996]. Without any empirical parameters and coefficients, equation (B4) provides an analytical solution for the LCL as a function of near-surface temperature (T_0) and humidity (q_0), which are assigned as the temperature (θ_{BL}) and humidity (q_{BL}) in the boundary layer in this study. This expression can be easily computed using numerical routines, and the Lambert W function has been implemented in many software applications such as Maple, GP, Matlab, and Mathematica.

To obtain the altitude of the LCL, one needs to transfer the pressure level to the height level by assuming atmosphere in hydrostatic equilibrium. This one-to-one pressure-altitude relationship can be obtained from (A11) and (A12) by approximating the temperature profiles below the LCL as dry adiabatic profiles,

$$P(z) = P_0 \left(\frac{T(z)}{T_0} \right)^{-\frac{g}{RT_{dry}}}, \quad (B5)$$

with (B5), the altitude of the LCL can be transferred from equations (B4),

$$z_{LCL} = -\frac{T_0}{\Gamma_{dry}} + \frac{\lambda R}{g R_V W \left[\frac{\lambda R \Gamma_{dry}}{g R_V T_0} \left(\frac{P_0 q_0}{e_{ref}} \right)^{-\frac{RT_{dry}}{g}} \exp \left(\frac{\lambda R \Gamma_{dry}}{g R_V T_{ref}} \right) \right]}. \quad (B6)$$

Acknowledgments

We acknowledge the financial support from National Aeronautics and Space Administration (NASA grant NNX09AN76G), National Science Foundation (NSF-CBET-10-33467, NSF-EAR-0838301, NSF-EAR-1331846, and NSF-EAR-1316258), the U.S. Department of Energy through the Office of Biological and Environmental Research, Terrestrial Carbon Processes program (DE-SC0006967), USDA Agricultural Research Service (58-6408-3-027), as well as the Agriculture and Food Research Initiative from the U.S. Department of Agriculture (2011-67003-30222). Data were obtained from the Atmospheric Radiation Measurement Program sponsored by the U.S. Department of Energy (available from <http://www.arm.gov/>). We thank the Editor, Associate Editor, and two anonymous reviewers for useful suggestions and encouragement. Models used in the paper are available upon request.

References

- Ball, F. K. (1960), Control of inversion height by surface heating, *Q. J. R. Meteorol. Soc.*, *86*(370), 483–494, doi:10.1002/qj.49708637005.
- Ball, J. T., I. E. Woodrow, and J. A. Berry (1987), A model predicting stomatal conductance and its contribution to the control of photosynthesis under different environmental conditions, in *Progress in Photosynthesis Research*, edited by J. Biggins, pp. 221–224, Springer, Netherlands.
- Bartlett, M. S., G. Vico, and A. Porporato (2014), Coupled carbon and water fluxes in CAM photosynthesis: Modeling quantification of water use efficiency and productivity, *Plant Soil*, *383*(1–2), 111–138.
- Battan, L. J. (1973), *Radar Observation of the Atmosphere*, Univ. of Chicago Press, Chicago, Ill.
- Betts, A. K. (1973), Non-precipitating cumulus convection and its parameterization, *Q. J. R. Meteorol. Soc.*, *99*(419), 178–196, doi:10.1002/qj.49709941915.
- Betts, A. K. (2009), Land-surface-atmosphere coupling in observations and models, *J. Adv. Model. Earth Syst.*, *1*, 4, doi:10.3894/JAMES.2009.1.4.
- Betts, A. K., J. H. Ball, A. C. M. Beljaars, M. J. Miller, and P. A. Viterbo (1996), The land surface-atmosphere interaction: A review based on observational and global modeling perspectives, *J. Geophys. Res.*, *101*(D3), 7209–7225, doi:10.1029/95JD02135.
- Bonetti, S., G. Manoli, J.-C. Domec, M. Putti, M. Marani, and G. G. Katul (2015), The influence of water table depth and the free atmospheric state on convective rainfall predisposition, *Water Resour. Res.*, *51*, 2283–2297, doi:10.1002/2014WR016431.
- Borland, A. M., H. Griffiths, J. Hartwell, and J. A. C. Smith (2009), Exploiting the potential of plants with crassulacean acid metabolism for bio-energy production on marginal lands, *J. Exp. Bot.*, *60*(10), 2879–2896, doi:10.1093/jxb/erp118.
- Bretherton, C. S., M. E. Peters, and L. E. Back (2004), Relationships between water vapor path and precipitation over the tropical oceans, *J. Clim.*, *17*(7), 1517–1528.
- Brubaker, K. L., and D. Entekhabi (1995), An analytic approach to modeling land atmosphere interaction: 1. Construct and equilibrium behavior, *Water Resour. Res.*, *31*(3), 619–632, doi:10.1029/94WR01772.
- Brutsaert, W. (1982), *Evaporation Into the Atmosphere: Theory, History and Applications*, 299 pp., Springer, Dordrecht, Netherlands.
- Brutsaert, W. (1998), Land-surface water vapor and sensible heat flux: Spatial variability, homogeneity, and measurement scales, *Water Resour. Res.*, *34*(10), 2433–2442, doi:10.1029/98WR01340.
- Brutsaert, W. (2005), *Hydrology: An Introduction*, Cambridge Univ. Press, N. Y.

- Burke, C. J. (1945), Transformation of polar continental air to polar maritime air, *J. Meteorol.*, 2(2), 94–112, doi:10.1175/1520-0469(1945)002<0094:TOPCAT>2.0.CO;2.
- Carson, D. J. (1973), The development of a dry inversion-capped convectively unstable boundary layer, *Q. J. R. Meteorol. Soc.*, 99(421), 450–467, doi:10.1002/qj.49709942105.
- Chandra, A. S., P. Kollias, S. E. Giangrande, and S. A. Klein (2010), Long-term observations of the convective boundary layer using insect radar returns at the SGP ARM climate research facility, *J. Clim.*, 23(21), 5699–5714, doi:10.1175/2010JCLI3395.1.
- Clapp, R. B., and G. M. Hornberger (1978), Empirical equations for some soil hydraulic-properties, *Water Resour. Res.*, 14(4), 601–604, doi:10.1029/WR014i004p00601.
- Corless, R. M., G. H. Gonnet, D. E. G. Hare, D. J. Jeffrey, and D. E. Knuth (1996), On the Lambert W function, *Adv. Comput. Math.*, 5(1), 329–359, doi:10.1007/BF02124750.
- D’Oroico, P., and A. Porporato (2004), Preferential states in soil moisture and climate dynamics, *Proc. Natl. Acad. Sci. U. S. A.*, 101(24), 8848–8851, doi:10.1073/pnas.0401428101.
- Daly, E., A. Porporato, and I. Rodriguez-Iturbe (2004), Coupled dynamics of photosynthesis, transpiration, and soil water balance. Part I: Upscaling from hourly to daily level, *J. Hydrometeorol.*, 5(3), 546–558, doi:10.1175/1525-7541(2004)005<0546:CDOPTA>2.0.CO;2.
- Dean, A. R., R. S. Schneider, R. L. Thompson, J. Hart, and P. D. Bothwell (2009), The conditional risk of severe convection estimated from archived NWS/Storm Prediction Center mesoscale objective analyses: Potential uses in support of forecast operations and verification, paper presented at 23rd Conference on Weather Analysis and Forecasting/19th Conference on Numerical Weather Prediction, Am. Meteorol. Soc., Omaha, Nebr.
- Ek, M., and L. Mahrt (1994), Daytime evolution of relative humidity at the boundary-layer top, *Mon. Weather Rev.*, 122(12), 2709–2721, doi:10.1175/1520-0493(1994)122<2709:DEORHA>2.0.CO;2.
- Ek, M. B., and A. A. M. Holtlag (2004), Influence of soil moisture on boundary layer cloud development, *J. Hydrometeorol.*, 5(1), 86–99, doi:10.1175/1525-7541(2004)005<0086:IOSMOB>2.0.CO;2.
- Emanuel, K. A. (1994), *Atmospheric Convection*, Oxford Univ. Press, N. Y.
- Findell, K. L., and E. A. B. Eltahir (2003), Atmospheric controls on soil moisture–boundary layer interactions. Part I: Framework development, *J. Hydrometeorol.*, 4(3), 552–569, doi:10.1175/1525-7541(2003)004<0552:ACOSML>2.0.CO;2.
- Findell, K. L., P. Gentile, B. R. Lintner, and C. Kerr (2011), Probability of afternoon precipitation in eastern United States and Mexico enhanced by high evaporation, *Nat. Geosci.*, 4(7), 434–439, doi:10.1038/ngeo1174.
- Ford, T. W., A. D. Rapp, and S. M. Quiring (2014), Does afternoon precipitation occur preferentially over dry or wet soils in Oklahoma?, *J. Hydrometeorol.*, 16(2), 874–888, doi:10.1175/JHM-D-14-0005.1.
- Garratt, J. R. (1992), *The Atmospheric Boundary Layer*, Cambridge Univ. Press, Cambridge, U. K.
- Gentile, P., A. A. M. Holtlag, F. D’Andrea, and M. Ek (2013), Surface and atmospheric controls on the onset of moist convection over land, *J. Hydrometeorol.*, 14(5), 1443–1462, doi:10.1175/JHM-D-12-0137.1.
- Guillod, B. P., B. Orlowsky, D. G. Miralles, A. J. Teuling, and S. I. Seneviratne (2015), Reconciling spatial and temporal soil moisture effects on afternoon rainfall, *Nat Commun.*, 6, 6443, doi:10.1038/ncomms7443.
- Hartzell, S., M. S. Bartlett, L. Virgin, and A. Porporato (2015), Nonlinear dynamics of the CAM circadian rhythm in response to environmental forcing, *J. Theor. Biol.*, 368(0), 83–94, doi:10.1016/j.jtbi.2014.12.010.
- Jarvis, P. G. (1976), The interpretation of the variations in leaf water potential and stomatal conductance found in canopies in the field, *Philos. Trans. R. Soc. London B*, 273(927), 593–610, doi:10.1098/rstb.1976.0035.
- Juang, J.-Y., A. Porporato, P. C. Stoy, M. S. Siqueira, A. C. Oishi, M. Detto, H.-S. Kim, and G. G. Katul (2007a), Hydrologic and atmospheric controls on initiation of convective precipitation events, *Water Resour. Res.*, 43(3), W03421, doi:10.1029/2006WR004954.
- Juang, J.-Y., G. G. Katul, A. Porporato, P. C. Stoy, M. S. Siqueira, M. Detto, H.-S. Kim, and R. Oren (2007b), Eco-hydrological controls on summertime convective rainfall triggers, *Global Change Biol.*, 13(4), 887–896, doi:10.1111/j.1365-2486.2006.01315.x.
- Katul, G., R. Leuning, and R. Oren (2003), Relationship between plant hydraulic and biochemical properties derived from a steady-state coupled water and carbon transport model, *Plant Cell Environ.*, 26(3), 339–350, doi:10.1046/j.1365-3040.2003.00965.x.
- Kirkpatrick, C., E. W. McCaul Jr., and C. Cohen (2011), Sensitivities of simulated convective storms to environmental CAPE, *Mon. Weather Rev.*, 139(11), 3514–3532, doi:10.1175/2011MWR3631.1.
- Konings, A. G., G. G. Katul, and A. Porporato (2010), The rainfall-no rainfall transition in a coupled land-convective atmosphere system, *Geophys. Res. Lett.*, 37, L14401, doi:10.1029/2010GL043967.
- Koster, R. D., M. J. Suarez, R. W. Higgins, and H. M. Van den Dool (2003), Observational evidence that soil moisture variations affect precipitation, *Geophys. Res. Lett.*, 30(5), 1241, doi:10.1029/2002GL016571.
- Koster, R. D., et al. (2004), Regions of strong coupling between soil moisture and precipitation, *Science*, 305(5687), 1138–1140, doi:10.1126/science.1100217.
- Lilly, D. K. (1968), Models of cloud-topped mixed layers under a strong inversion, *Q. J. R. Meteorol. Soc.*, 94(401), 292–309, doi:10.1002/qj.49709440106.
- Lüttge, U. (2000), The tonoplast functioning as the master switch for circadian regulation of crassulacean acid metabolism, *Planta*, 211(6), 761–769, doi:10.1007/s004250000408.
- McNaughton, K. G., and T. W. Spriggs (1986), A mixed-layer model for regional evaporation, *Boundary Layer Meteorol.*, 34(3), 243–262, doi:10.1007/BF00122381.
- Neelin, J. D., O. Peters, and K. Hales (2009), The transition to strong convection, *J. Atmos. Sci.*, 66(8), 2367–2384, doi:10.1175/2009JAS2962.1.
- Phillips, T. J., and S. A. Klein (2014), Land-atmosphere coupling manifested in warm-season observations on the U.S. southern great plains, *J. Geophys. Res. Atmos.*, 119, 509–528, doi:10.1002/2013JD020492.
- Pielke, R. A., et al. (2011), Land use/land cover changes and climate: Modeling analysis and observational evidence, *WIREs Clim. Change*, 2(6), 828–850, doi:10.1002/wcc.144.
- Pitman, A. J. (2003), The evolution of, and revolution in, land surface schemes designed for climate models, *Int. J. Climatol.*, 23(5), 479–510, doi:10.1002/joc.893.
- Porporato, A. (2009), Atmospheric boundary-layer dynamics with constant Bowen ratio, *Boundary Layer Meteorol.*, 132(2), 227–240, doi:10.1007/s10546-009-9400-8.
- Porporato, A., and P. D’Oroico (2004), Phase transitions driven by state-dependent Poisson noise, *Phys. Rev. Lett.*, 92(11), 110601, doi:10.1103/PhysRevLett.92.110601.
- Qian, Y., M. Huang, B. Yang, and L. K. Berg (2013), A modeling study of irrigation effects on surface fluxes and land–air–cloud interactions in the Southern Great Plains, *J. Hydrometeorol.*, 14(3), 700–721, doi:10.1175/JHM-D-12-0134.1.

- Rodríguez-Iturbe, I., and A. Porporato (2005), *Ecohydrology of Water-Controlled Ecosystems: Soil Moisture and Plant Dynamics*, Cambridge Univ. Press, Cambridge, U. K.
- Scanlon, T. M., and J. D. Albertson (2004), Canopy scale measurements of CO₂ and water vapor exchange along a precipitation gradient in southern Africa, *Global Change Biol.*, *10*(3), 329–341, doi:10.1046/j.1365-2486.2003.00700.x.
- Siqueira, M., G. Katul, and A. Porporato (2009), Soil moisture feedbacks on convection triggers: The role of soil–plant hydrodynamics, *J. Hydrometeorol.*, *10*(1), 96–112, doi:10.1175/2008JHM1027.1.
- Stage, S. A., and J. A. Businger (1981), A model for entrainment into a cloud-topped marine boundary layer. Part I: Model description and application to a cold-air outbreak episode, *J. Atmos. Sci.*, *38*(10), 2213–2229, doi:10.1175/1520-0469(1981)038<2213:AMFEIA>2.0.CO;2.
- Stevens, B. (2006), Bulk boundary-layer concepts for simplified models of tropical dynamics, *Theor. Comput. Fluid Dyn.*, *20*(5–6), 279–304.
- Stull, R. B. (1976), The energetics of entrainment across a density interface, *J. Atmos. Sci.*, *33*(7), 1260–1267, doi:10.1175/1520-0469(1976)033<1260:TEOEAD>2.0.CO;2.
- Stull, R. B. (1988), *An Introduction to Boundary Layer Meteorology*, Kluwer Acad., Dordrecht, Netherlands.
- Taylor, C. M., R. A. M. de Jeu, F. Guichard, P. P. Harris, and W. A. Dorigo (2012), Afternoon rain more likely over drier soils, *Nature*, *489*(7416), 423–426, doi:10.1038/nature11377.
- Tennekes, H. (1973), A model for the dynamics of the inversion above a convective boundary layer, *J. Atmos. Sci.*, *30*(4), 558–567, doi:10.1175/1520-0469(1973)030<0558:AMFTDO>2.0.CO;2.
- Tsonis, A. A. (2002), *An Introduction to Atmospheric Thermodynamics*, Cambridge Univ. Press, Cambridge, U. K.
- Vico, G., and A. Porporato (2008), Modelling C3 and C4 photosynthesis under water-stressed conditions, *Plant Soil*, *313*(1–2), 187–203.
- Westra, D., G. J. Steeneveld, and A. A. M. Holtslag (2012), Some observational evidence for dry soils supporting enhanced relative humidity at the convective boundary layer top, *J. Hydrometeorol.*, *13*(4), 1347–1358, doi:10.1175/JHM-D-11-0136.1.
- Yin, J., A. Porporato, and J. Albertson (2014), Interplay of climate seasonality and soil moisture-rainfall feedback, *Water Resour. Res.*, *50*, 6053–6066, doi:10.1002/2013WR014772.
- Zhang, G. J. (2009), Effects of entrainment on convective available potential energy and closure assumptions in convection parameterization, *J. Geophys. Res.*, *114*, D07109, doi:10.1029/2008JD010976.
- Zhang, G. J., and N. A. McFarlane (1991), Convective stabilization in midlatitudes, *Mon. Weather Rev.*, *119*(8), 1915–1928, doi:10.1175/1520-0493(1991)119<1915:CSIM>2.0.CO;2.
- Zhang, G. J., and N. A. McFarlane (1995), Sensitivity of climate simulations to the parameterization of cumulus convection in the Canadian Climate Centre general circulation model, *Atmos. Ocean*, *33*(3), 407–446.
- Zhang, G. J., and X. Song (2009), Interaction of deep and shallow convection is key to Madden-Julian Oscillation simulation, *Geophys. Res. Lett.*, *36*, L09708, doi:10.1029/2009GL037340.